

# UC Irvine

## UC Irvine Previously Published Works

### Title

Transformation of spatial sensitivity along the ascending auditory pathway

### Permalink

<https://escholarship.org/uc/item/23b9g06d>

### Journal

Journal of Neurophysiology, 113(9)

### ISSN

0022-3077

### Authors

Yao, Justin D  
Bremen, Peter  
Middlebrooks, John C

### Publication Date


2015-05-01

### DOI

10.1152/jn.01029.2014

Peer reviewed

## Transformation of spatial sensitivity along the ascending auditory pathway

Justin D. Yao,<sup>1,3</sup>  Peter Bremen,<sup>2,3</sup> and John C. Middlebrooks<sup>1,2,3,4,5</sup>

<sup>1</sup>Department of Neurobiology and Behavior, University of California at Irvine, Irvine, California; <sup>2</sup>Department of Otolaryngology, University of California at Irvine, Irvine, California; <sup>3</sup>Center for Hearing Research, University of California at Irvine, Irvine, California; <sup>4</sup>Department of Cognitive Sciences, University of California at Irvine, Irvine, California; <sup>5</sup>Department of Biomedical Engineering, University of California at Irvine, Irvine, California

Submitted 18 December 2014; accepted in final form 27 February 2015

**Yao JD, Bremen P, Middlebrooks JC.** Transformation of spatial sensitivity along the ascending auditory pathway. *J Neurophysiol* 113: 3098–3111, 2015. First published March 5, 2015; doi:10.1152/jn.01029.2014.—Locations of sounds are computed in the central auditory pathway based primarily on differences in sound level and timing at the two ears. In rats, the results of that computation appear in the primary auditory cortex (A1) as exclusively contralateral hemifield spatial sensitivity, with strong responses to sounds contralateral to the recording site, sharp cutoffs across the midline, and weak, sound-level-tolerant responses to ipsilateral sounds. We surveyed the auditory pathway in anesthetized rats to identify the brain level(s) at which level-tolerant spatial sensitivity arises. Noise-burst stimuli were varied in horizontal sound location and in sound level. Neurons in the central nucleus of the inferior colliculus (ICc) displayed contralateral tuning at low sound levels, but tuning was degraded at successively higher sound levels. In contrast, neurons in the nucleus of the brachium of the inferior colliculus (BIN) showed sharp, level-tolerant spatial sensitivity. The ventral division of the medial geniculate body (MGB<sub>v</sub>) contained two discrete neural populations, one showing broad sensitivity like the ICc and one showing sharp sensitivity like A1. Dorsal, medial, and shell regions of the MGB showed fairly sharp spatial sensitivity, likely reflecting inputs from A1 and/or the BIN. The results demonstrate two parallel brainstem pathways for spatial hearing. The tectal pathway, in which sharp, level-tolerant spatial sensitivity arises between ICc and BIN, projects to the superior colliculus and could support reflexive orientation to sounds. The lemniscal pathway, in which such sensitivity arises between ICc and the MGB<sub>v</sub>, projects to the forebrain to support perception of sound location.

spatial hearing; medial geniculate body; inferior colliculus; lemniscal; tectal

SPATIAL HEARING PERMITS a listener to determine the locations of sound sources based on spatial cues derived from the interaction of sound with the head and external ears. Those cues are processed in specialized brainstem nuclei, and the output of those nuclei converges in the central nucleus of the inferior colliculus (ICc) (Grothe et al. 2010). Multisynaptic pathways from the ICc reach two structures in which neurons exhibit spatial sensitivity: the superior colliculus (SC) and the auditory cortex. It is unknown from the published literature whether spatial sensitivity arises *de novo* at the levels of the SC and auditory cortex by convergence of pathways representing individual spatial cues or whether that spatial sensitivity is inherited from such a convergence at a lower level of the auditory pathway.

Address for reprint requests and other correspondence: J. Middlebrooks, Dept. of Otolaryngology, Univ. of California, Irvine. Medical Sciences E, Rm. E116 Univ. of California, Irvine, Irvine, CA 92697-5310 (e-mail: j.middlebrooks@uci.edu).

The tectal pathway projects from the ICc to the SC by way of the nucleus of the brachium of the inferior colliculus (BIN) (Jiang et al. 1993; King et al. 1998; Nodal et al. 2005; Slee and Young 2013). Note that the BIN is the nucleus of the brachium, a cell group that lies adjacent to the brachium itself; the brachium is the major fiber bundle containing the axons of ICc principal cells. Topographical representations of auditory space based on space-tuned neurons have been described in the SC of anesthetized guinea pigs, cats, and ferrets (King and Hutchings 1987; Middlebrooks and Knudsen 1984; Palmer and King 1982). The lemniscal pathway projects by way of the medial geniculate body (MGB) to the primary auditory cortex, area A1. Area A1 in carnivores and primates exhibits a variety of spatial sensitivity, including spatially insensitive omnidirectional responses, contralateral hemifield tuning, and, in a minority of neurons, frontal and ipsilateral tuning (King and Middlebrooks 2011).

In anesthetized rats, essentially all neurons in A1 studied with free-field stimulation show level-tolerant contralateral-hemifield spatial sensitivity consisting of strong responses to sounds contralateral to the recording site, a sharp cutoff in responses across the midline, and weak responses to ipsilateral sounds (Yao et al. 2013). Consistent with the finding of exclusively hemifield spatial sensitivity, a study in rat A1 using dichotic stimulation found primarily excitatory/inhibitory responses (Kyweriga et al. 2014). That study concluded that the excitatory/inhibitory responses were inherited from subcortical processing, consistent with our findings in the present study. The Kyweriga group also studied a second class of binaural responses, predominantly binaural. Those neurons were found primarily in the rat's suprarhinal auditory field, and their responses were determined to reflect intracortical processing.

The rat lacks the variety of spatial sensitivity that is seen in primates and carnivores. For that reason, it is an ideal animal model for study of the most common form of spatial sensitivity observed across species, contralateral hemifield tuning, because, in examining subcortical structures in the rat, one can be confident of the spatial sensitivity of target neurons in area A1. We also note that the spatial tuning seen in the rat's area A1 coincides with the rat's performance in psychophysical tasks, in which it discriminates sounds on the left from those on the right of the midline with reasonable spatial acuity but fails to discriminate locations within one hemifield (Kavanaugh and Kelly 1986).

The present study surveyed spatial sensitivity in the auditory pathway of the anesthetized rat with the goal of identifying the first location(s) of level-tolerant spatial sensitivity. We quantified the spatial sensitivity of neurons in the ICc, the BIN, and

structures of the MGB including the ventral (MBGv), medial (MGBm), and dorsal (MGBd) divisions and the shell nucleus (MGBs), and we compared those data with our previous data from area A1 (Yao et al. 2013). The results show that level-tolerant contralateral hemifield spatial sensitivity arises independently in tectal and lemniscal pathways. Surprisingly, we found two distinct populations of neurons in the MGBv, distinguished only by their spatial sensitivity. It remains to be tested whether those MGBv populations represent two stages in a progression from broad to sharp spatial sensitivity or whether they are components of parallel broadly and sharply sensitive pathways.

## MATERIALS AND METHODS

We recorded from IC and MGB neurons in 14 adult male Sprague-Dawley rats (median age: 11.1 wk; Charles River Laboratories, Hollister, CA) weighing 265–475 g (median weight: 380 g) and compared these data with previously reported data from cortical area A1 in 15 other rats (Yao et al. 2013). All procedures were performed with the approval of the University of California at Irvine Institutional Animal Care and Use Committee according to the National Institutes of Health guidelines and were largely identical to those of a previous report from our laboratory (Yao et al. 2013). In what follows, we briefly describe the procedures with an emphasis on differences between our previous cortical and the current subcortical recordings.

### *Animal Surgery*

Surgical anesthesia was induced with urethane (1.5 g/kg ip) and xylazine (10 mg/kg ip) and supplemented as needed to maintain an areflexive state. To reduce the viscosity of bronchial secretions and to prevent brain edema, we administered atropine sulfate (0.1 mg/kg ip) and dexamethasone (0.25 mg/kg ip), respectively, at the beginning of surgery and every 12 h thereafter. Core body temperature was maintained at  $\sim 37^{\circ}\text{C}$ .

Surgery began with a midline scalp incision and the exposure of the underlying skull. We cemented an inverted machine screw to the skull on the midline, rostral to bregma, to serve as a head holder. The skull was opened as needed to access the right IC and MGB. Before recordings, the scalp was partially closed, and the positions of the pinnae were adjusted to minimize any alteration the surgical procedure may have caused. Recordings were made with multisite recording probes (described below). The right ICc and BIN were accessed with vertical probe placements (14 placements in 5 animals)  $\sim 2$ – $3$  mm lateral to the midline and  $\sim 7$ – $9$  mm caudal to bregma. Two approaches were used to access the right MGB. The vertical approach (22 probe placements in 8 animals) used vertical probe placements  $\sim 3$ – $4$  mm lateral to the midline and  $\sim 5$ – $6$  mm caudal to bregma. The lateral approach (18 probe placements in 6 animals) used a dorso-lateral to ventro-medial trajectory,  $\sim 30$ – $50^{\circ}$  from the sagittal plane,  $\sim 4$ – $6$  mm caudal to bregma.

### *Experimental Setup, Stimulus Generation, and Data Acquisition*

The animal was positioned in the center of a darkened double-walled sound-attenuating chamber (inside dimensions  $2.6 \times 2.6 \times 2.5$  m; Industrial Acoustics, Bronx, NY) that was lined with 60-mm-thick absorbent foam (SONEXone, Seattle, WA). The animal's head was supported by a 10-mm-diameter rod attached to the skull screw. The rod was held by a thin metal frame positioned behind the animal. The area around the head and ears was unobstructed.

We used Tucker-Davis Technologies System 3 equipment (Alachua, FL) controlled by a personal computer running custom MATLAB (MathWorks, Natick, MA) scripts for stimulus generation and data

acquisition. Sounds were presented one at a time from 18 two-way coaxial loudspeakers (8.4-cm diameter; Pioneer Electronics, Long Beach, CA) that were located 1.2 m from the rat's head. The loudspeakers were positioned in the horizontal plane aligned to the interaural axis of the animal and were spaced  $20^{\circ}$  apart. We express loudspeaker locations in degrees of azimuth relative to the loudspeaker directly located in front of the animal's head ( $0^{\circ}$ ). Negative values indicate locations on the animal's left, contralateral to the recording side located on the animal's right. We calibrated the loudspeakers individually to flatten and equalize their frequency responses (Zhou et al. 1992) using a precision microphone positioned in the center of the sound chamber at the normal position of the rat's head; the rat was absent during the calibration. The addition of the rat's ear-canal resonance added some gain at the level of the tympanic membrane relative to the level in the sound field (average gain of  $24.1 \pm 3.3$  dB at 17.2 kHz; Koka et al. 2008), and there was an additional gain of  $\sim 10$  dB attributed to diffraction by the rat's head and pinna at the particular speaker location of  $-40^{\circ}$ , at which thresholds were measured. The reported minimum thresholds of  $-10$  dB sound pressure level (SPL) at specific characteristic frequencies (CFs), therefore, are equivalent to  $\sim 20$  dB SPL in the ear canal, depending on frequency.

We recorded extracellular spike activity with single-shank silicon-substrate multisite recording probes from NeuroNexus Technologies (Ann Arbor, MI) using high-impedance head stages and multichannel amplifiers (Tucker-Davis Technologies). The probes had either 16 recording sites spaced at  $100\text{-}\mu\text{m}$  intervals or 32 sites spaced at  $50\text{-}\mu\text{m}$  intervals; recording-site areas were  $177\ \mu\text{m}^2$ . Neural waveforms were digitized at 24.4 k samples/s and stored on computer disk for offline analysis.

### *Experimental Procedure*

The vertical approach to the IC typically encountered sound-evoked unit activity at a depth 3–6 mm below the surface of the occipital cortex. The probe depth was adjusted to maximize the number of recording sites with stimulus-evoked spiking activity. Typically, sustained or strong-onset neural spike activity was seen on all sites. In the vertical approach to the MGB, we typically encountered stimulus-evoked activity at a depth of  $\sim 5$ – $6.5$  mm below the cortical surface. In the lateral approach to the MGB, we first encountered neural spiking activity at depths of  $\sim 1$  mm as the probe first advanced through auditory cortical fields. This initial auditory activity ceased at a depth of  $\sim 2$  mm. Stimulus-evoked activity returned at a depth of about 5–6.5 mm, indicating that the electrode had reached the MGB. We adjusted the probe depth to maximize the number of recording sites with stimulus-evoked spiking activity. Following probe placement, the exposed brain tissue was covered with warmed 2% agarose dissolved in Ringer's solution. The agarose cooled to form a gel that reduced brain pulsations and kept the exposed brain surface moist.

At each probe placement, we first recorded frequency response areas (FRAs) with pure tones presented from the loudspeaker at  $-40^{\circ}$ . Tones were 80 ms in duration with 5-ms raised-cosine onset and offset ramps. Tones varied in frequency from 0.2 to 40.0 kHz in 1/3- or 1/6-octave steps and in level in 10-dB steps, typically from  $-10$  to 60 or 70 dB SPL with 10 repetitions per frequency-level combination. We next recorded mean spike rate vs. azimuth functions (RAFs) to 80-ms Gaussian noise bursts across  $360^{\circ}$  in azimuth in  $20^{\circ}$  steps and at levels ranging from  $-10$  to 70 dB SPL in 10-dB steps (20 repetitions per combination). All stimuli were presented at a repetition rate of 1.00 or 1.25/s. Data collection for the present study took  $\leq 75$  min at each probe placement. Additional stimuli needed for another study also were tested, extending the recording session at a single probe placement to between  $\sim 2$  and 5 h, with experiments lasting  $\sim 18$ – $20$  h.

### Assignment of Units to IC and MGB Subdivisions

Units were localized to ICc and BIN based on stereotaxic coordinates of probe placements and response properties. Localization of probe placements was confirmed histologically in a subset of cases. Units localized in the ICc typically displayed sustained responses to pure tones and broadband noise, sharp frequency tuning, and a dorsal-to-ventral low-to-high gradient of characteristic frequency (Malmierca et al. 2008). BIN units were typically encountered when probe placements were made at more rostral (~1–2 mm) and slightly lateral (<~1 mm) sites relative to ICc penetrations and caudal (~2 mm) from the probe placements made in the MGB. The BIN was studied with one probe placement in each of three rats and with two placements, separated rostrocaudally by 0.5 to 1.0 mm, in each of two other rats. Consistent with published reports in other species, units localized in the BIN displayed first-spike latencies comparable to those of ICc units, strong onset responses but rarely sustained firing, relatively broad frequency tuning, and a lack of a clear tonotopic gradient (Schnupp and King 1997; Slee and Young 2013).

Unit localization within the subdivisions of the MGB was based on physiological criteria of spike patterns, latency, and frequency response properties that were consistent with previous reports in small mammals (rat: Bordi and LeDoux 1994a, 1994b; Edeline et al. 1999; guinea pig: Anderson et al. 2007; He 2001; He and Hu 2002; mouse: Anderson and Linden 2011; Hackett et al. 2011; gerbil: Bäuerle et al. 2011); again, locations of a subset of probe placements were confirmed histologically. A total of 363 MGBv units were studied: 193 from vertical probe placements and 170 from lateral placements. Sharp “primary-like” or V-shaped frequency tuning and a lateral-to-medial increase in CFs (lateral approach) were taken as signatures of the MGBv. The MGBm was accessed exclusively using the lateral approach (41 units). The functional boundary from the MGBv to the MGBm was given by an increase in frequency bandwidth and a reversal in the CF gradient upon entering MGBm. The MGBd and MGBs were encountered most often using vertical probe placements (83/98 MGBd units; 48/60 MGBs units). The boundary from the MGBd to the MGBv was marked by a reduction in first-spike latency and a sharpening of frequency tuning. MGBs units were distinguished by their long first-spike latency and were typically encountered when probe placements were made at more lateral sites relative to MGBv penetrations.

The positions of 11 of the 54 probe placements (6 IC and 11 MGB) were verified histologically in 10 rats. For that purpose, the rear side of the silicon probes was coated with 4-(4-(dihexadecylamino)styryl)-*N*-methylpyridinium iodide (DiA), which is a lipophilic aminostyryl dye (DiCarlo et al. 1996). The DiA inserts itself readily into cell membranes and exhibits a strong fluorescence (~580 nm). After the conclusion of these experiments, animals were perfused with 4% paraformaldehyde and the brains sectioned on a vibratome. Sections were counterstained with DAPI (D-1306; Invitrogen, Carlsbad, CA). Fluorescent images were photographed, stored, and adjusted for brightness and contrast using Adobe Photoshop. We were able to recover 11 electrode tracks (4 in IC and 7 in MGB) from a total of 17 coated probe placements (Fig. 1). The locations of probes seen in the histology agreed well with the locations inferred from stereotaxic coordinates and response properties.

### Data Analysis

**Spike sorting.** All quantitative analyses are based on neuronal action potentials identified with an offline spike-sorting procedure that is similar to the one previously used in our laboratory (Middlebrooks 2008). First, a denoising procedure was applied to simultaneously recorded analog waveforms to attenuate signals that were common to multiple recording sites (Bierer and Anderson 1999). Putative action potentials were next extracted using a root-mean-squared-based threshold-crossing procedure. The selected peaks then were sorted

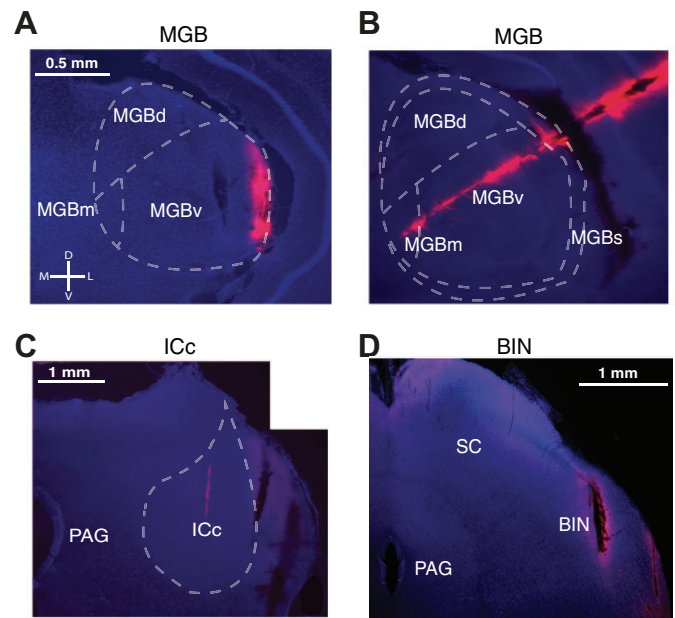


Fig. 1. Histological reconstruction of recording sites in 4 animals (coronal view). **A:** vertical approach to the medial geniculate body (MGB) (FF1309). MGBv, ventral division of the MGB; MGBd, dorsal division; MGBm, medial division. **B:** lateral approach to the MGB (FF1402). MGBs, shell division. **C:** vertical approach to the inferior colliculus (IC) (FF1401). ICc, central nucleus of the IC; PAG, periaqueductal gray. **D:** vertical approach to the BIN (FF1403). The rear sides of the recording probes were coated with 4-(4-(dihexadecylamino)styryl)-*N*-methylpyridinium iodide (red) to determine their anatomical position. Sections were counterstained with DAPI (blue). SC, superior colliculus; BIN, brachium of the inferior colliculus.

using an algorithm based on *k*-means clustering of the first three principal components of the putative action potentials. Visual inspection of waveforms and measures of mean spike counts verified the stability of recordings during the  $\leq 75$  min needed to collect the FRA and the RAF. We report spike times corrected for the 3.5-ms acoustic travel time between the loudspeaker and the animal’s head (Yao et al. 2013) and latencies based on responses to CF at highest level. For units with unclear CFs (80 total), latencies were taken as the shortest first-spike latencies across all tested frequencies at the highest level.

Responses were classified as well-isolated single units when they showed 1) uniform waveform appearance upon visual inspection, 2) interspike intervals that revealed a clear refractory period  $> 1$  ms, and 3) stability of spike amplitude during the  $\leq 75$ -min recording period. According to that classification, our sample of well-isolated single units consisted of 31 units in the IC and 55 in the MGB. An additional 246 recordings in the IC and 507 recordings in the MGB were classified as multiple units consisting of unresolved spikes from two or more neurons. Analysis of relative spike times on adjacent pairs of electrode sites showed little or no indication of spikes being recorded on multiple sites. We did not observe differences between properties calculated from the single compared with multiple units across any measure of spatial sensitivity at any suprathreshold level ( $K = 0.17–0.35$ ,  $P = 0.09–0.78$ , 2-sample Kolmogorov-Smirnov test). The lack of differences between single and multiple units suggests that the variance in stimulus sensitivity among neurons recorded as a multiple unit was small enough that there was no broadening of apparent sensitivity compared with that of single neurons. In summary illustrations, the range and percentiles of distributions of multiunit responses are represented by boxes and whiskers, and well-isolated single units are represented by individual symbols. By every measure, every single-unit response fell within the range of multiunit responses. For those reasons, we combined single- and multiple-unit data in statistical tests of populations, and we use the term unit to refer to both

well-isolated and unresolved recordings. The unit count did not include the 75 units in the IC and 135 in the MGB that we excluded from the analysis because they responded with less than an average of one spike per trial to their most effective stimulus or with a maximum spike rate less than two standard deviations above their spontaneous rates.

*Frequency response area, characteristic frequency, spectral bandwidth, and noise-burst threshold.* We extracted frequency-tuning curves (FTCs) from the measured FRAs using procedures described in signal detection theory (Green and Swets 1966; Macmillan and Creelman 2005; Middlebrooks and Snyder 2007). For each frequency-level combination and all repetitions, we accumulated the trial-by-trial distributions of spike counts and constructed an empirical receiver-operator-characteristic (ROC) curve for the stimulus condition vs. a nonstimulus condition (i.e., vs. a silent interval of the same duration) as a measure of spontaneous rate. The area under the ROC curve gave the proportion of trials in which one condition elicited more spikes than the other one. We expressed this proportion as a  $z$ -score multiplied by  $\sqrt{2}$  to yield the discrimination index,  $d'$ . A  $d'$  of 1 indicates a one-standard-deviation separation of the means of the two distributions (stimulus vs. silent). A stimulus thus elicited activity above spontaneous rate if it yielded a  $d' \geq 1$ .

For each unit, the matrix of  $d'$  values across all tested frequencies and levels was screened to eliminate isolated values of  $d' > 1$  for which all neighboring values were  $< 1$ ; this eliminated isolated values lying outside the FRA. The FTC (i.e., the border of the FRA) was then found by interpolating the  $d'$  values across all tested sound levels in 1-dB steps at each tested frequency and finding the minimum sound level at which  $d' \geq 1$ . The CF was given by the frequency of the lowest-level tip of the FTC. The filter bandwidth was estimated by fitting a rounded symmetrical exponential filter (roex-filter; Patterson 1976) to the FTC as follows:

$$|H(f)|^2 = (1 + Pg)e^{-Pg} \quad (1)$$

where  $g$  is the normalized deviation of the frequency from the CF,  $P$  is the slope parameter, and  $|H(f)|^2$  represents the squared magnitude of the filter. The slope parameter  $P$  can be used to calculate the equivalent rectangular bandwidth (ERB) as:

$$\text{ERB} = 4CF/P \quad (2)$$

ERB represents the bandwidth of a rectangular filter whose area is equal to that of the FTC and takes the entire FTC into account. The  $Q_{\text{ERB}}$  (Verschooten et al. 2012) was computed to provide a value of sharpness of tuning normalized across CFs:

$$Q_{\text{ERB}} = CF/\text{ERB} \quad (3)$$

The thresholds for detection of neural activity elicited by noise bursts were computed by ROC analysis of trial-by-trial spike counts on trials in which a noise burst was or was not present. The minimum noise level eliciting  $d' > 1$ , interpolated in 1-dB steps, was taken as the noise-burst threshold.

*Measures of spatial sensitivity.* An ROC procedure also was used to quantify discrimination between pairs of stimulus locations based on spike counts. On the basis of responses to noise bursts at a fixed sound level, we found the trial-by-trial distribution of spike counts to noise bursts at a particular source location and compared that with the corresponding distribution for every other source location. The ROC analysis yielded a value of  $d'$  for each of the 153 unique combinations of 18 source locations. A discrimination index (DI) was given by the number of pairwise comparisons yielding  $d' \geq 1$  divided by 153. A DI of 0.5, for example, would indicate that half of the pairwise comparisons of source locations could be discriminated significantly by the spike rate of a neuron.

The breadth of spatial sensitivity by each unit was represented by the width of its equivalent rectangular receptive field (ERRF) (Lee and Middlebrooks 2011; Yao et al. 2013). The ERRF width was

computed by integrating the area under the RAF of a unit, forming a rectangle having peak height and area equal to that of the RAF, and measuring the resulting width.

The preferred stimulus location of each unit was represented by its spatial centroid (Middlebrooks et al. 1998; Yao et al. 2013). Spatial centroids were computed only for neurons that showed  $\geq 50\%$  modulation of their mean spike rates by sound-source location across a  $360^\circ$  range. To obtain the spatial centroid, we first identified the peak of the RAF by finding the range of one or more contiguous locations that elicited spike rates  $\geq 75\%$  of the maximum spike rate; we also included the two neighboring locations having rates below that criterion. The spatial centroid was given by the orientation of the spike-rate-weighted vector sum across source locations within the peak.

The location in azimuth at which the response of a neuron was most strongly modulated by source location was given by the steepest slope of its RAF. The steepest slope location of each neuron was computed by convolving its RAF with a  $40^\circ$  boxcar window, calculating the first derivative of mean spike rate with azimuth, and then finding the azimuth at which the slope was maximal.

Many units showed a broadening of their spatial sensitivity with increasing sound level. We quantified that for each unit by fitting a least-squares regression line to its ERRF widths in degrees vs. sound levels in dB. The slope of each such fit was taken as a measure of level dependence.

*Measures of distinct patterns of spatial sensitivity in MGBv.* We noted fairly uniform spatial sensitivity properties within the ICc and within A1, whereas there were marked differences between ICc and A1. The population of recordings from MGBv, in contrast, exhibited a variety of spatial sensitivity, with some units showing broad spatial sensitivities like that seen in the ICc and others showing sharp spatial sensitivity like that seen in A1. We tested whether the similarity to ICc vs. similarity to A1 formed a continuum or whether there were functionally distinct populations. That test consisted of comparing the RAF of each MGBv unit to templates of RAFs of ICc and A1 units; all the comparisons used responses to sounds 40 dB above unit thresholds. The templates were formed by normalizing the RAF of each ICc or A1 unit by its peak value and then computing the mean across all ICc units (using data from the present study) or across all A1 units (using data from our previous study; Yao et al. 2013). The RAF of each MGBv unit was compared with the two templates by computing the Euclidean distance (ED):

$$\text{ED}_T = \sqrt{\sum_{\theta}^n (R_{\theta} - T_{\theta})^2} \quad (4)$$

where  $R$  is the RAF of one MGBv unit,  $T$  is the ICc or A1 template,  $\theta$  is the source location in azimuth, and  $n$  is the number of tested source locations (18). We then computed for each MGBv unit a similarity index (SI):

$$\text{SI} = \text{ED}_{\text{ICc}} / (\text{ED}_{\text{ICc}} + \text{ED}_{\text{A1}}) \quad (5)$$

where  $\text{ED}_{\text{ICc}}$  and  $\text{ED}_{\text{A1}}$  indicate the EDs from the ICc and A1 templates, respectively. An SI value close to 1 indicates that the individual test unit is more similar to the A1 template, and an SI value close to 0 indicates greater similarity to the ICc template.

The template-matching procedure demonstrated distinct populations of ICc-like and A1-like units in the MGBv, as presented in RESULTS. We tested whether there was any anatomical segregation of those populations, analogous to the segregation in other species that has been demonstrated using connective techniques (cat: Middlebrooks and Zook 1983; Read et al. 2008; rabbit: Cetas et al. 2002). We used a permutation analysis to test for a nonrandom distribution of units in MGBv with similar spatial sensitivity (Ernst 2004; Middlebrooks and Bremen 2013). For each multisite recording-probe placement, we counted the number of adjacent pairs of recording sites at which units showed similar spatial sensitivity. For example, a run of A1-like responses at three consecutive sites would be counted as two

matched pairs. We then totaled the number of recording sites yielding A1-like and ICc-like responses across all recordings in the MGBv. We also formed a list of the number of recording sites in the MGBv on each of the 34 probe placements. For each permutation, we distributed all the MGBv units randomly across virtual probes having the same number of sites as the actual probe placements and counted the number of matching adjacent pairs of units. That procedure was repeated for 100,000 permutations, each time with a different random distribution of response types across virtual probes. The actual number of matching adjacent recordings was compared with the distribution of numbers of matching pairs across the permutations. If the actual recorded number of matching pairs was greater than the maximum value obtained across all permutations, the probability of obtaining that actual number by chance was taken as  $<10^{-5}$ .

**Tests of statistical hypotheses.** We used custom-written MATLAB scripts (MathWorks) that incorporated the MATLAB Statistics Toolbox when appropriate. All post hoc multiple comparisons used the Bonferroni correction. We used a goodness-of-fit measure (D'Agostino's  $K^2$  test) to test whether a given data set was normally distributed. We report median and interquartile values and used non-parametric statistical tests on data sets for which a given measure was not normally distributed. In addition, we used the two-sample Kolmogorov-Smirnov goodness-of-fit hypothesis test to check for statistically significant difference between two population samples. In the text, distributions are summarized by 25th, 50th, and 75th percentiles, written as  $-/-/-$ .

## RESULTS

We present data from a total of 839 single- and multi-unit recordings in 14 animals: 277 units in 14 probe placements in the IC and 562 units in 40 probe placements in the MGB. Of the 277 IC units studied, 146 (53%) were localized to the ICc, and 131 (47%) were localized to the BIN. Of the 562 MGB units, 363 (65%) were localized to the MGBv, 98 (17%) to the MGBd, 41 (7%) to the MGBm, and 60 (11%) to the MGBs. Figure 1 depicts coronal sections through the MGB (Fig. 1, A and B) and the IC (Fig. 1, C and D) from four animals. The dashed white lines indicate the approximate borders of the subdivisions of each structure based on the appearance of the tissue and on stereotaxic coordinates (Paxinos and Watson 2005). The orange-red fluorescent DiA traces indicate the electrode tracks. The sections in Fig. 1, A and B, were taken  $\sim 5.5$  and  $\sim 5.8$  mm posterior to bregma, respectively. The labeled tracks are seen passing through the MGBv (Fig. 1, A and B) and entering the MGBm (Fig. 1B). The section in Fig. 1C was taken  $\sim 8.8$  mm posterior to bregma and contains the ICc. The section in Fig. 1D was taken  $\sim 7.5$  mm posterior to bregma and contains the SC and BIN. The labeled track in Fig. 1C passes through the ICc, whereas the labeled track in Fig. 1D is located in the region designated as the BIN.

### Frequency Tuning

Across our samples of ICc and BIN units, CFs ranged from 1 to  $>32$ ;  $>32$  denotes instances in which CFs were higher than the 32-kHz maximum tested frequency. The quartiles of the CF distribution in the ICc were 7.17/12.7/26.7 kHz and in the BIN were 11.1/27.3/ $>32$  kHz. The distribution of CFs in the BIN was shifted significantly toward higher frequencies than that in the ICc ( $K = 0.32$ ,  $P < 10^{-6}$ ; 2-sample Kolmogorov-Smirnov test). Units localized to the ICc typically displayed sharp frequency tuning (Fig. 2A;  $\text{ICc}_{\text{QERB}}$ : 0.74/1.00/1.24), whereas frequency tuning of BIN units was significantly

broader (Fig. 2D;  $\text{BIN}_{\text{QERB}}$ : 0.61/0.93/1.13;  $K = 0.15$ ,  $P = 0.038$ ; 2-sample Kolmogorov-Smirnov test). We overestimated  $\text{QERB}$  (i.e., underestimated bandwidths) in some cases because many FRAs appeared to extend to frequencies higher than 32 kHz, which was the highest that we tested; that was a greater problem in BIN than ICc because of the higher-frequency FRAs in BIN. The ICc displayed a tonotopic frequency gradient, with low and high CFs located dorsally and ventrally, respectively. The quartiles of CF range between the most superficial and deepest electrode sites along individual vertical probe placements in the ICc were 2.15/2.70/4.10 octaves. The tonotopic gradient was less pronounced within the BIN; CF ranges between the most superficial and deepest electrode sites were distributed with quartiles of only 0.35/1.09/1.65 octaves, and there was no evident progression of CFs among recording sites on individual probes. The observation in the rat of broader frequency tuning in the BIN than in the ICc generally agrees with previous observations in the ferret (Schnupp and King 1997) and marmoset (Slee and Young 2013).

Figure 2, G and J, shows FRAs from two isolated single units in the MGBv with CFs of 26 and 21 kHz, respectively. Across our sample of MGBv units, CFs ranged from 1 to  $>32$  kHz (10.2/20.4/ $>32$  kHz). Frequency tuning in our sample of MGBv units was slightly but significantly broader than that observed in the ICc ( $\text{MGBv}_{\text{QERB}}$ : 0.85/0.98/1.12; MGBv vs. ICc  $K = 0.16$ ,  $P = 0.010$ ; 2-sample Kolmogorov-Smirnov test) and sharper than that in the BIN ( $K = 0.17$ ,  $P = 0.0044$ ; 2-sample Kolmogorov-Smirnov test). The three nonlemniscal MGB nuclei all showed broad, nonprimary-like frequency tuning (Fig. 3, A, D, and G;  $\text{MGBd}_{\text{QERB}}$ : 0.59/0.73/1.01;  $\text{MGBm}_{\text{QERB}}$ : 0.51/0.86/1.03;  $\text{MGBs}_{\text{QERB}}$ : 0.50/0.85/1.06).  $\text{QERB}$  values differed significantly among MGB subdivisions [ $\chi^2_{(3,546)} = 22.6$ ,  $P < 10^{-5}$ ; Kruskal-Wallis]. Bonferroni-corrected multiple comparisons indicated significant differences between MGBv and MGBd, MGBv and MGBm, and MGBv and MGBs ( $P < 0.05$ ) with MGBm displaying the broadest frequency tuning (proportion of  $\text{QERB} < 1$ , MGBv: 40%; MGBd: 56%; MGBm: 69%; MGBs: 58%). The calculation of CF and  $\text{QERB}$  was difficult in the nonlemniscal nuclei, especially in the MGBd, because of the nonprimary-like FTCs (e.g., Fig. 3A). For that reason, we were able to compute these measures in only 58% of MGBd units and 33% of MGBs units. For the nonlemniscal units where calculation of CF was successful, values ranged from 1 to  $>32$  kHz ( $\text{MGBd}_{\text{CF}}$ : 10.1/12.3/25.2;  $\text{MGBm}_{\text{CF}}$ : 7.17/10.1/22.3;  $\text{MGBs}_{\text{CF}}$ : 11.7/24.4/ $>32$ ).

### First-Spike Latencies

We measured first-spike latencies of all units using stimuli at the highest sound level tested at unit CF. In units for which we were not able to extract a CF (1 ICc, 8 BIN, 72 MGBd, and 22 MGBs), we recorded the shortest latency observed across all tested frequencies at the highest level. First-spike latencies in the BIN (8.62/9.27/10.2 ms) were slightly but significantly longer than those in the ICc (8.49/8.86/9.81 ms;  $K = 0.15$ ,  $P = 0.047$ ; 2-sample Kolmogorov-Smirnov test). The small median latency difference ( $<0.50$  ms) between these structures is somewhat unexpected given that the ICc is presynaptic to the BIN (Nodal et al. 2005), but we note that similarly small differences have been reported previously in the marmoset

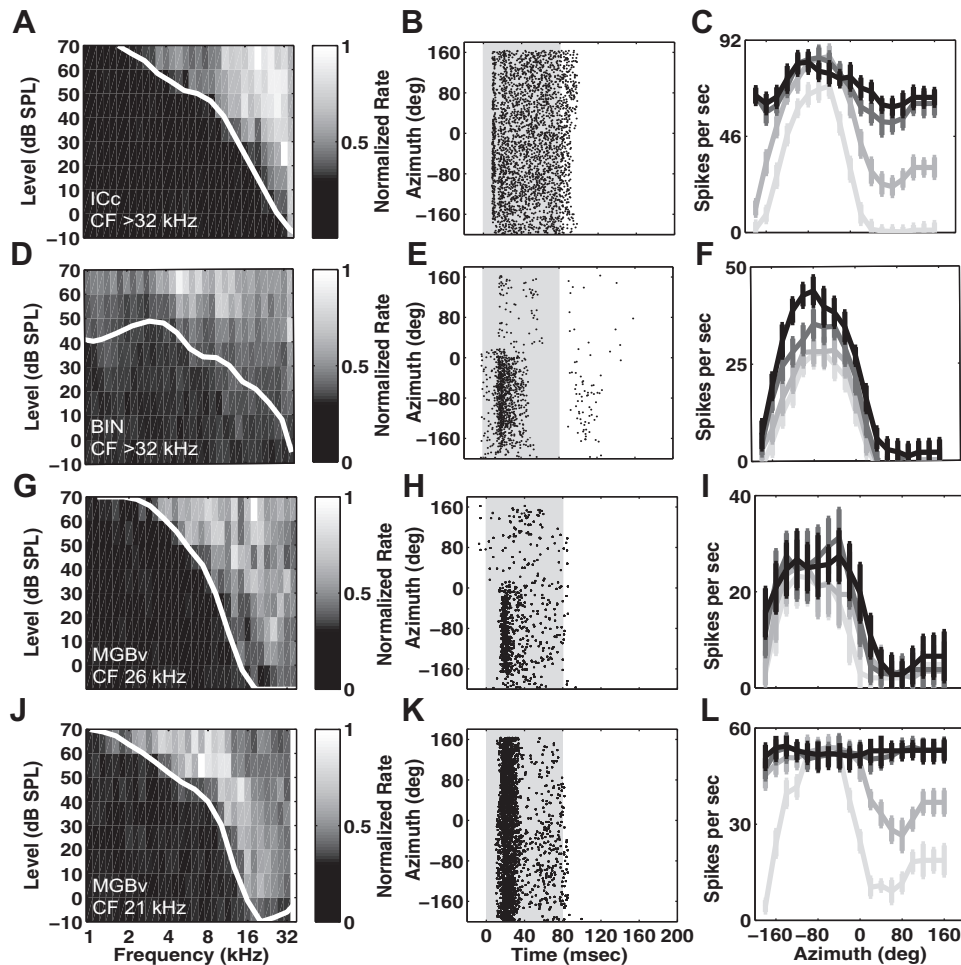


Fig. 2. Examples of neural responses from well-isolated single units in rat ICc (A–C) (1403.5.31), BIN (D–F) (1404.7.32), and MGBv (G–L) (1312.4.21 and 1404.5.5). The left column (A, D, G, and J) displays frequency response areas plotted as the normalized spike rate in response to pure-tone stimulation varying in frequency (x-axis) and sound level (y-axis). White lines represent extracted frequency-tuning curves (3-point running average for visual purposes). The middle column (B, E, H, and K) displays dot rasters of spike times (x-axis) elicited by noise stimuli at 40 dB above the threshold of the unit, varying in azimuth (y-axis). Each dot represents 1 spike. Gray shading represents the stimulus duration. The right column (C, F, I, and L) displays rate-azimuth functions (RAFTs) of spike rate (spike count/s) plotted against stimulus azimuth locations at levels 10, 20, 30, and 40 dB above threshold and corrected for spontaneous rate. Error bars indicate standard error of the mean. Characteristic frequencies (CFs) are indicated for each example unit. SPL, sound pressure level.

(Slee and Young 2013). In general, the short latencies seen among our sampled midbrain units suggest that we did not record from other nuclei within the IC, such as the dorsal cortex, which contains units with much longer latencies (Syka et al. 2000; Lumani and Zhang 2010).

Significant differences in first-spike latencies were seen among MGB subdivisions [ $\chi^2_{(3,579)} = 375$ ,  $P < 10^{-6}$ ; Kruskal-Wallis]. Consistent with being postsynaptic from the ICc, MGBv and MGBm showed roughly 1 ms longer first-spike latencies compared with the ICc (MGBv: 9.60/9.93/10.7 ms; MGBm: 9.77/10.2/11.6 ms). Those latency distributions (MGBv vs. MGBm) were not statistically different from each other ( $P > 0.05$ , Bonferroni corrected for multiple comparisons). First-spike latencies of MGBd (28.1/33.5/40.2 ms) and MGBs (36.3/42.5/45.1 ms) units, however, were substantially longer compared with those of MGBv and MGBm units ( $P < 10^{-6}$ , Bonferroni corrected), consistent with their classification as being part of nonlemniscal and/or corticofugal pathways.

### Spiking Patterns

Examples of the various spiking patterns that were encountered are given in the middle column of panels in Figs. 2 and 3. Each of these dot raster plots represents responses to noise bursts at 40 dB above unit thresholds. The vertical axis of each plot represents the full range of tested sound-source azimuth. As illustrated by the example in Fig. 2B, units in the ICc displayed a strong onset and sustained spiking pattern. In

contrast, BIN units responded phasically and typically lacked the sustained component seen among ICc units (Fig. 2E). Spike patterns for each ICc and BIN unit were quantified with the same response index used by Slee and Young (2013) in which the difference in spike rate between the first (0–40 ms) and second half (41–80 ms) of the stimulus duration is divided by the sum of both halves. This index ranges from  $-1$  (build up response) to  $1$  (purely phasic response). An index value of  $0$  indicates a purely sustained response. Index response values for all BIN units were  $>0$  (5th percentile, 0.25) and typically clustered around 0.80 (median, 0.78), whereas ICc units possessed index response values near  $0$  (median, 0.18; significantly different from BIN units,  $P < 10^{-6}$ ; rank sum). The prevalence of phasic responses in the BIN compared with the ICc is consistent with findings in the BIN of anesthetized ferrets (Schnupp and King 1997) although the majority of units in the BIN in awake marmosets (Slee and Young 2013) show sustained responses. This difference might be attributable to the use of anesthetics in the ferret and present study.

MGBv and MGBm units typically responded phasically to the onsets of the stimuli (Figs. 2, H and K, and 3E). MGBd units responded selectively to sound-source locations within the contralateral hemifield and responded phasically to these locations (Fig. 3B). Units localized in the MGBs exhibited strong onset responses, with some units showing additional sustained or offset responses (Fig. 3H).

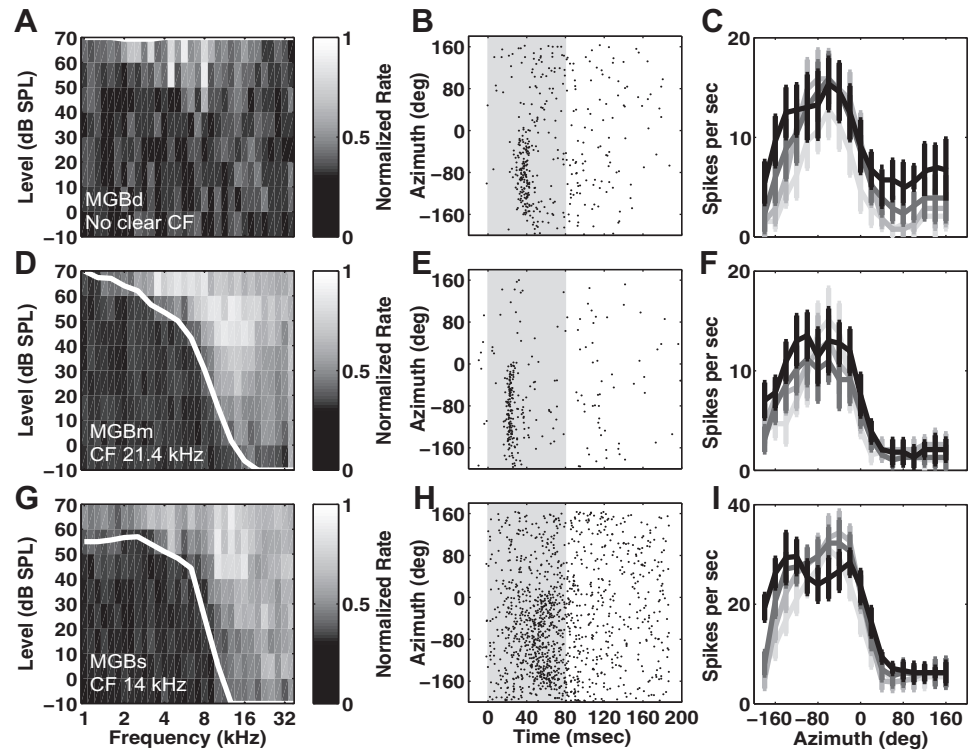


Fig. 3. Examples of neural responses of well-isolated single units in rat MGBd (A–C) (1403.7.12), MGBm (D–F) (1302.6.15), and MGBs (G–I) (1404.1.32). All conventions as in Fig. 2.

### Offset Responses

We noticed weak location-specific offset responses in 19 of 146 (13%) units in the ICc and 23 of 131 (18%) units in the BIN; offset responses typically occurred  $>10$  ms after stimulus offset (ICc: 10.5/11/13.7 ms; BIN: 11/11.5/17.9 ms). For ICc units with offset responses, 13/19 (68%) responded only to  $+80^\circ$  (among the locations tested in  $20^\circ$  increments), whereas the rest (6/19, 32%) were specific to  $-60^\circ$ . Offset responses from all BIN units (23/23, 100%) were specific to  $+80^\circ$ . The distribution of units showing offset responses along each probe placement within the ICc and BIN tended to be random, with no instance of more than two neighboring sites showing offset responses.

We observed offset responses in a small proportion of MGBv units (25/363; 7%). These offset responses typically occurred  $\sim 20$  ms after stimulus offset (17.1/20.5/22.1 ms) and were seen across multiple azimuth locations. Of these units, 80% (20/25) were driven by ipsilateral locations, whereas the remaining units (5/25) showed stronger offset responses to contralateral locations. Only two units in the MGBm (4.8%) displayed offset responses. Those responses were to ipsilateral locations and occurred  $\sim 15$ – $20$  ms after stimulus onset. A greater number of offset responses was seen within the MGBd (38/98; 38.8%) with latencies typically occurring  $\sim 21$  ms after stimulus offset (10/21/35.5 ms). Of the 38 units, 3 (7.9%) showed equal responses to all locations, 26 (68.4%) showed stronger responses to ipsilateral locations, and 9 (23.7%) showed stronger responses to contralateral locations. Within the MGBs, 33.3% (20/60) of units displayed offset responses. These offset responses occurred  $\sim 20$  ms (20/20.8/22 ms) with 80% (16/20) of these units showing stronger offset responses to ipsilateral locations and the rest showing stronger responses to contralateral locations.

Units exhibiting offset responses tended to form clusters within specific MGB subdivisions. Of the 15 adjacent pairs of sites across 12 multisite probe placements that displayed offset responses in the MGBv, 14 (93.3% of pairs) showed matching responses. Of the 27 pairs of sites in the MGBd with offset responses, 26 (96.3%) showed matching responses. In the MGBs, 10/12 (83.3%) adjacent pairs of sites showed matching offset responses. Our results are consistent with the offset response pathways seen in the MGB of the guinea pig, where neurons with offset responses typically formed clusters along the outer edges of the MGBv and within neighboring subdivisions like the MGBd and MGBs (He 2001).

### Examples of Spatial Sensitivity

The spatial sensitivity of units from various IC and MGB subdivisions is represented by well-isolated single units shown in the right column of panels in Figs. 2 and 3. Spike rates (spikes/s) as a function of azimuth location (RAFs) are plotted for sound levels 10, 20, 30, and 40 dB above unit threshold (shades of gray, darkness increasing with sound level); error bars indicate standard errors of the mean. The example ICc unit (Fig. 2C) showed spatial sensitivity primarily for contralateral sources when sound levels were only 10 dB above unit threshold. That spatial sensitivity was markedly degraded, however, at higher sound levels, primarily because of increases in the responses to ipsilateral sound sources. In contrast to ICc units, units in the BIN exhibited sharp spatial sensitivity across all levels tested. This can be seen in the example BIN unit in Fig. 2F, which responded selectively to contralateral sound sources and showed little or no response to ipsilateral sources, regardless of sound level. The example MGBv unit depicted in Fig. 2I also responded in a level-tolerant manner, responding selectively to sources in the contralateral hemifield. Spatial sensitivity of the second example MGBv unit (Fig. 2L) was



much more vulnerable to increasing sound levels, similar to responses of ICc units. Units in the other MGB subdivisions (Fig. 3, C, F, and I) generally showed sharp, sound-level-tolerant contralateral tuning similar to that shown by BIN units (Fig. 2F) and by the more spatially sensitive MGBv units (Fig. 2I).

#### Two Physiologically Distinct Subpopulations in the MGBv

We observed two patterns of spatial sensitivity among units in the MGBv. One pattern consisted of sharp, level-tolerant contralateral specificity like that illustrated in Fig. 2I and like we have encountered in cortical area A1 (Yao et al. 2013), and the other consisted of broader spatial sensitivity that degraded with increasing sound levels like that illustrated in Fig. 2L and like we observed in the ICc. We tested whether the two patterns of spatial specificity, sharp vs. broad, represented extremes of a continuum or whether they were characteristic of two functionally distinct neural populations. For that purpose, we developed a template-matching procedure in which we compared the RAF of each MGBv unit with two templates, one based on a grand mean of RAFs of cortical area A1 units measured in our previous study (Yao et al. 2013) and the other based on a grand mean of RAFs of ICc units measured in the present study; the template-matching procedure is detailed in MATERIALS AND METHODS. All of the RAFs used for that analysis were those measured at the highest tested sound level, 40 dB above unit thresholds. Figure 4A illustrates the A1 template (thick line and filled circles), the ICc template (thick line and X markers) and an RAF of one MGBv unit (thin line and open circles).

Our template-matching procedure yielded an SI that could range from 0 to 1, where numbers nearer 0 indicate greater

similarity to the ICc and numbers nearer 1 indicate greater similarity to A1. The distribution of SI values from all MGBv units is plotted in Fig. 4B. There was a clear bimodal distribution (dip = 0.06,  $P < 10^{-6}$ ; Hartigan's dip test) with peaks at around 0.30 and 0.70, consistent with the view that MGBv consists of two classes of units distinguished by their spatial sensitivity. We classified units having SI values  $< 0.50$  or  $\geq 0.50$  as ICc-like or A1-like, respectively. The individual normalized RAFs of MGBv units that were classified in that way are illustrated in Fig. 4C ( $n = 129$  ICc-like units) and Fig. 4D ( $n = 234$  A1-like units). We also compared the RAF of each BIN unit with the two A1 and ICc templates. Consistent with our impressions of BIN spatial tuning, the distribution of SI values from all BIN units was unimodal, with each of 131 units possessing an SI value  $> 0.50$  (median, 0.63).

We tested whether the two populations of MGBv that were distinguished by their spatial sensitivity differed in other response properties; specifically, we compared distributions of CF, breadth of frequency tuning (i.e.,  $Q_{\text{ERB}}$ ), and first-spike latency. Figure 5, A and B, displays frequency bandwidth ( $Q_{\text{ERB}}$ ) and first-spike latency of the two populations as a function of unit CF in one-octave bins. Within each ICc-like or A1 group, the  $Q_{\text{ERB}}$  increased (i.e., frequency tuning narrowed) with increasing CF [ICc-like:  $X^2_{(5,123)} = 31.9$ ,  $P < 10^{-5}$ ; A1-like:  $X^2_{(5,228)} = 83.8$ ,  $P < 10^{-6}$ ; Kruskal-Wallis]. Within each one-octave CF band, however, there was no significant difference between ICc-like and A1-like groups ( $P = 0.15\text{--}0.97$ ; rank sum). Neither ICc-like nor A1-like groups showed a significant dependence of first-spike latency on CF [ICc-like:  $X^2_{(5,123)} = 10.1$ ,  $P = 0.07$ ; A1-like:  $X^2_{(5,228)} = 3.99$ ,  $P = 0.55$ ; Kruskal-Wallis]. All but one of the one-octave CF bands showed no significant difference between groups

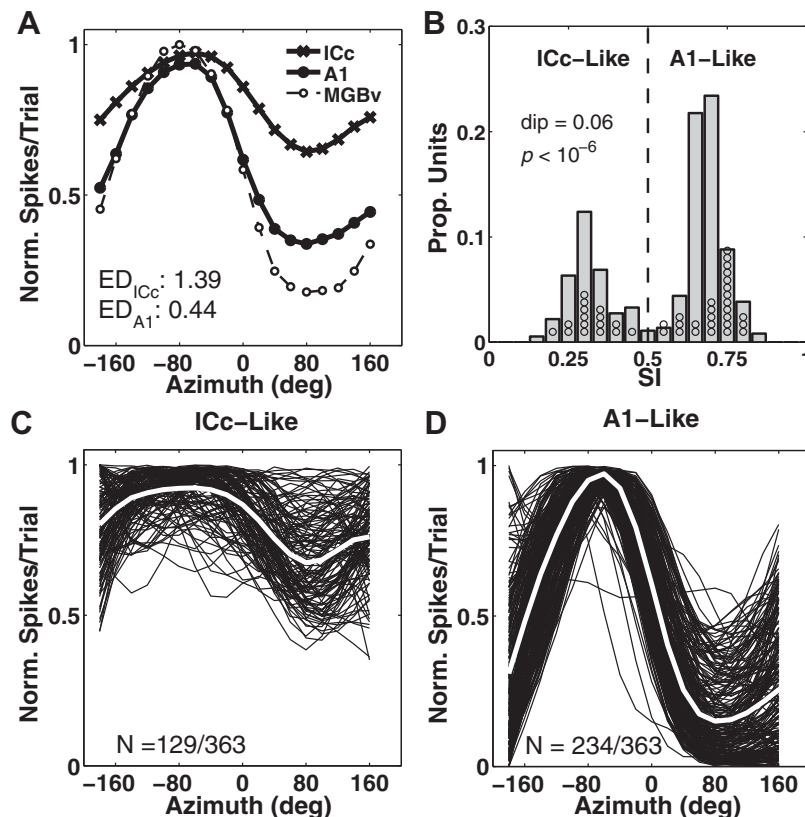


Fig. 4. Classifying distinct classes of spatial sensitivity in MGBv. *A*: normalized RAF at 40 dB above unit threshold from 1 example MGBv unit (thin line and  $\circ$ ) overlaid with RAF templates constructed from all ICc (thick line and x markers) and A1 (thick line and  $\bullet$ ) units. Euclidean distance (ED) values between the example MGBv RAF and templates are indicated in the panel. ED values were used to calculate the similarity index (SI). These metrics were used to determine how closely each MGBv unit matches either template. *B*: distribution of SI values for all MGBv units. Circles represent data from single units. Vertical dashed line represents the boundary at 0.50. Dip statistics and corresponding  $P$  value are indicated in the panel. *C* and *D*: individual MGBv RAFs assigned as ICc-like (*C*) and A1-like (*D*). White lines represent the grand means.

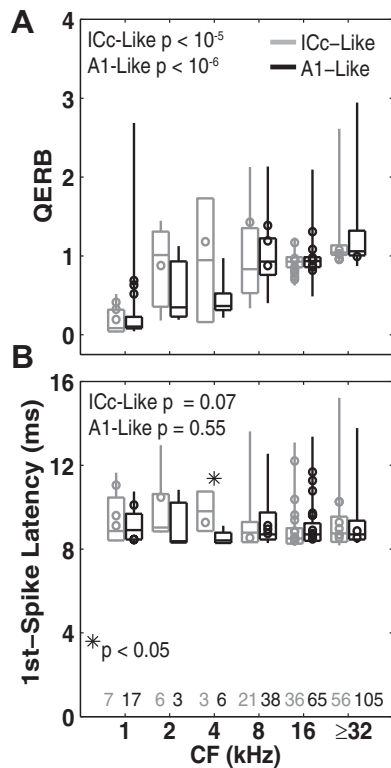


Fig. 5. Distribution of equivalent rectangular bandwidth (ERB)  $Q_{ERB}$  values (A) and first-spike latencies (B) from ICc-like (gray) and A1-like (black) units in the MGBv plotted as a function of unit CF binned at 1-octave bands. Horizontal lines forming the boxes indicate the 25th, 50th, and 75th percentiles of multiunit responses. Vertical lines indicate the full range from multiunit responses. Circles represent data points from well-isolated single units.  $P$  values (Kruskal-Wallis) are indicated in the panel. The row of numbers above the horizontal axis indicates the total number of units represented in each bin.

( $P = 0.26-0.88$ , rank sum). The exception was the band centered on 4 kHz ( $P = 0.04$ , rank sum), but we doubt the importance of that difference given the small numbers of units in those groups.

We tested for a correlation between SI and unit CF by performing a Spearman rank-correlation analysis with 10,000 bootstrapped replications. For each replication, we randomly drew with replacement an equal number of units per one-octave CF bin from the MGBv population. Confidence intervals (CIs) were calculated from each distribution of correlation coefficients (empirical 2-tailed). No relationship was seen

between SI and unit CF [correlation coefficient  $CI = (-0.20, 0.29)$ ,  $P > 0.05$ ; Spearman-rank correlation]. To summarize, the two unit populations that formed such a strikingly bimodal distribution on the basis of similar spatial sensitivity to ICc or A1 units showed little or no systematic difference in CF, sharpness of frequency tuning, or first-spike latency.

Within a single recording-probe placement in the MGBv, units at contiguous sequences of recording sites tended to fall within the same spatial sensitivity class. This led to the hypothesis that units that differed in spatial sensitivity were segregated anatomically within the MGBv. We tested that hypothesis by using a permutation test, which is detailed in MATERIALS AND METHODS. We examined 363 units along 40 multisite probe placements and counted 290 instances for which units at the 312 pairs of adjacent recording sites displayed matching spatial sensitivity classes. One hundred thousand random distributions of ICc- and A1-like units along 40 virtual recording probes yielded a median of 178 and a maximum of only 213 adjacent matching pairs. That the actual number of adjacent pairs was larger than the maximum across 100,000 permutations indicates a nonrandom distribution of response classes among recording sites at a level of  $P < 10^{-5}$ . There were 28 runs of 3–23 consecutive matching pairs of unit spatial sensitivity, spanning 150–1,150  $\mu\text{m}$ . The distribution of the lengths of runs of recording sites showing matching spatial sensitivity had quartiles of 200/350/600  $\mu\text{m}$ .

*Transformation of Spatial Sensitivity in the Ascending Pathway*

We quantified the breadth of spatial sensitivity by calculating ERRF widths (Fig. 6A) at all tested suprathreshold stimulus levels. Figure 6, A and B, plots data from all the studied brain regions plus the previously obtained data from cortical area A1 (Yao et al. 2013). Across all regions and levels tested, ERRF widths ranged from around 120° to around 300°, i.e., from somewhat less than a hemifield to covering nearly all azimuth locations. Generally, MGBv-A1-like units showed the narrowest ERRF widths, those in ICc and the MGBv-ICc-like population were broadest, and those of A1 units, BIN, and nonlemniscal MGB subdivisions were intermediate. The magnitudes of ERRF-width differences between regions varied with tested level, but the ranking in spatial sensitivity across regions remained nearly constant. Note that the difference in spatial sensitivity between MGBv-A1-like and MGBv-ICc-like units

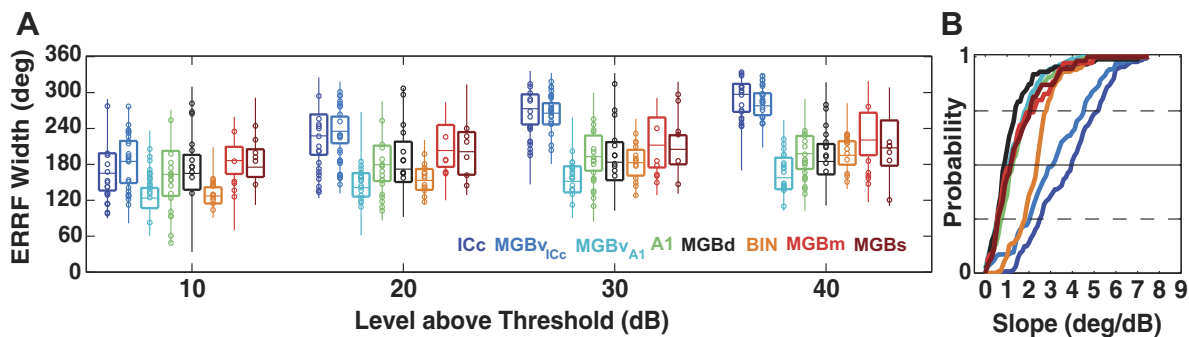


Fig. 6. Breadth of spatial sensitivity and level dependence. A: distributions of equivalent rectangular receptive field (ERRF) width grouped by the 4 tested sound levels above threshold for all sampled populations, as indicated by color. Horizontal lines forming the boxes indicate the 25th, 50th, and 75th percentiles of multiunit responses. Vertical lines indicate the full range from multiunit responses. Circles represent data points from well-isolated single units. B: cumulative distributions of linear fit slopes.

is expected, given that units in those groups were selected based on spatial tuning. Similarly, it is not surprising that median ERRF widths in A1 are broader than those in the MGBv-A1-like population given that the A1 population includes all A1 units that were encountered, whereas the MGBv-A1-like units were selected for sharp spatial tuning.

We found that all regions showed some variation in ERRF width with increasing level (Fig. 6A). ERRF widths for ICc and MGBv-ICc-like units increased most markedly with increasing level, with a median increase of 123° and 98°, respectively, between 10 and 40 dB above unit thresholds. All other regions were less susceptible to increasing levels, with median differences ranging from ~24° to ~34° between 10 and 40 dB above unit threshold for A1, MGBv-A1-like, and nonlemniscal MGB nuclei. BIN units showed a slightly greater change in ERRF width with increasing level, possessing a median increase of 69° between 10 and 40 dB above unit threshold. We fitted regression lines to the ERRF width vs. sound level above threshold functions on a unit-by-unit basis and used the slopes to quantify the dependence of sound level on spatial sensitivity. We present the cumulative distributions of slopes for all regions in Fig. 6B; this includes 168 units from A1 reported previously (Yao et al. 2013). We found that slopes differed significantly among all regions [ $X^2_{(7,999)} = 379.9$ ,  $P < 10^{-6}$ ; Kruskal-Wallis]. Specifically, ICc and MGBv-ICc-like units were most vulnerable to increasing levels, possessing the highest slopes ( $P < 10^{-6}$ ; post hoc multiple comparison, Bonferroni corrected), whereas A1 and nonlemniscal MGB units were least vulnerable. BIN units were slightly but significantly more vulnerable to increasing levels than A1 and nonlemniscal MGB units but less vulnerable (i.e., more level-tolerant) than ICc and MGBv-ICc-like units ( $P < 10^{-6}$ ; post hoc multiple comparison, Bonferroni-corrected). Overall, the most remarkable differences were between the ICc and its projection sites along the lemniscal (MGBv-A1-like) and tectal (BIN) pathways. These comparisons showed the greatest contrast in spatial sensitivity and level dependence. Thus the findings suggest that spatial sensitivity transforms along two independent pathways along the ascending auditory system with sharp, level-tolerant spatial sensitivity arising between the ICc and BIN as well as between the ICc and MGBv.

We compared our sampled populations across additional measures of spatial sensitivity, including preferred azimuth (represented by centroids) and steepest slope locations. Centroids were computed only for units that showed more than 50% modulation of their spike rates throughout 360° of azimuth; units showing less than that criterion for spike-rate modulation were classified as having no centroid (NC). The interquartile range from those centroids lay within 7.4 to 29.2° (left and right) of contralateral 60°, regardless of anatomical region or sound level. The percentage of NC units was highest among ICc and MGBv-ICc-like units at suprathreshold levels greater than 10 dB, and the percentages of NC units in those regions increased dramatically with increasing sound level. Steepest slope locations for BIN, A1, and units in all MGB nuclei except the MGBv-ICc-like units typically clustered within ~20° (interquartile range = -20 to 20°) of the midline across all levels. Steepest slope locations for MGBv-ICc-like and ICc units were vulnerable to increasing level, tending to shift ipsilaterally from the midline with increasing sound levels (interquartile range at 40 dB above threshold = -20 to 40°).

#### Discrimination of Sound-Source Locations

We tested how well individual units could distinguish between azimuth locations on the basis of trial-by-trial distributions of spike counts (described in MATERIALS AND METHODS and Yao et al. 2013). Figure 7, A–H shows examples from individual units as matrices of  $d'$  for all possible comparisons between azimuth locations at 40 dB above threshold; the examples correspond to the seven single units represented in Figs. 2 and 3 plus one area-A1 unit from our previous paper (Yao et al. 2013). Values of  $d' \geq 1$  indicate significant discrimination between the compared azimuth locations. These matrices are representative in that most BIN (Fig. 7A), MGBv-A1-like (Fig. 7B), A1 (Fig. 7C), MGBd (Fig. 7D), MGBm (Fig. 7G), and MGBs (Fig. 7H) units could readily discriminate between locations in differing hemifields, as indicated by high  $d'$  values in the upper left and lower right quadrants of the matrices but could not discriminate well within a hemifield. In contrast, most ICc (Fig. 7E) and MGBv-ICc-like (Fig. 7F) units could not discriminate reliably between any of the locations.

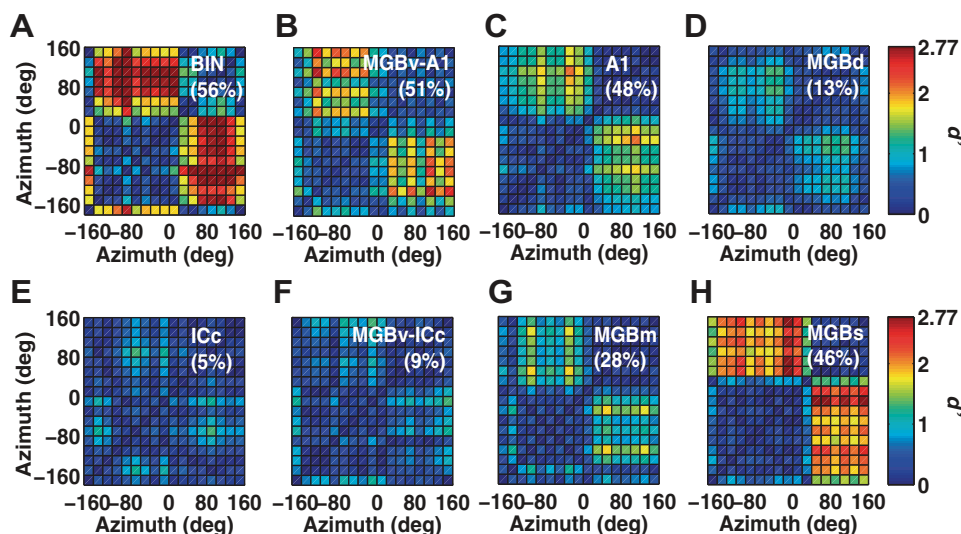


Fig. 7. Pairwise  $d'$  matrices for corresponding pairs of stimulus locations at 40 dB above threshold from the single units shown in Figs. 2 and 3. A: BIN. B: MGBv-A1-like. C: A1. D: MGBd. E: ICc. F: MGBv-ICc-like. G: MGBm. H: MGBs. Stimulus locations were separated by 20°. Significant discriminations among paired locations are indicated by  $d' \geq 1$ .

The overall accuracy of location discrimination by each unit was quantified by the percentage of location pairs that could be discriminated with  $d' \geq 1$ . In principle, this percentage could range from 0, meaning no locations discriminated, to 100, meaning all pairs of locations discriminated. On the basis of the typical sinusoidal shape of the RAFs of the most spatially sensitive units, however, one would expect the maximum percentage of discriminated location pairs to be closer to 50%, indicating discrimination of most between-hemifield location pairs and few discriminations within hemifields. Figure 8 plots the median and interquartile ranges of the percentages of discriminated location pairs from the various sampled regions as a function of level above threshold. The comparisons between sampled populations mirror the trends of ERRF-width measures in Fig. 6A. For instance, consistent with displaying the sharpest spatial sensitivity, MGBv-A1-like and BIN units possessed the highest percentages ( $\sim 50\%$ ) across all sound levels. In addition, units from the remaining sampled regions consistently maintained effective discrimination of many source locations across levels, except for ICc and MGBv-ICc-like units, which showed a dramatic decrease in percentages with increasing levels (Fig. 8).

## DISCUSSION

The present results demonstrate a transformation of spatial sensitivity along the ascending tectal and lemniscal auditory pathways, with RAFs dramatically sharpening and becoming more level tolerant from the ICc to the BIN and from the ICc to the MGBv. Neurons within nonlemniscal MGB subdivisions displayed spatial sensitivity that largely reflects putative inputs from A1 or BIN. Unexpectedly, we observed that the MGBv, the major thalamic structure in the lemniscal pathway, contains two distinct classes of neurons distinguished by their spatial sensitivity. These two classes might be related to known neuron classes described in the literature (e.g., de Venecia et al. 1995, 1998; Hashikawa et al. 1991) and need to be further examined.

### *Two Parallel Pathways for Auditory Space Processing*

The schematic diagram in Fig. 9 summarizes a tentative circuit for spatial processing observed in the present study, commencing at the level of the ICc. The circuit is based on reported anatomical connections and on the present observations of spatial sensitivity. Spatial sensitivity in each brain region is represented by grand-mean RAFs at four sound levels.

All of the nonlemniscal MGB structures in the present study showed fairly sharp, level-tolerant spatial sensitivity. The short-latency space-sensitive responses in the MGBm could

reflect its reported inputs from the BIN (Kudo et al. 1984). The longer-latency responses in the MGBd could reflect descending input via corticofugal projections from A1 (Bartlett et al. 2000; Hazama et al. 2004; Rouiller and Welker 1991; Shi and Cassell 1997; Winer et al. 2001). The MGBs has primarily been characterized in guinea pigs (Anderson et al. 2007; He 2001; He and Hu 2001; Redies et al. 1989) and is thought to receive direct input from the rostral half of the MGBv; we omit that connection in our drawing because of the relative lack of anatomical evidence available in the rat. The spatial sensitivity in MGBs is similar to that of the sharply tuned units in MGBv although a direct projection from MGBv to MGBs would not account for the long latency of neurons in the shell nucleus.

We find evidence for two parallel pathways showing sharp, level-tolerant spatial tuning, both originating with neurons showing broad spatial sensitivity in the ICc. Neurons in the ICc showed contralateral spatial sensitivity at low sound levels that degraded rapidly at increasing levels, primarily attributable to level-dependent increases in responses to ipsilateral locations. The lack of spatial sensitivity at moderate sound levels was reflected in the inability of ICc units to discriminate between azimuth locations (Fig. 8). The presence of broad, level-dependent spatial tuning in our sample of ICc units matches the omnidirectional and level-dependent class of ICc units reported in other animals (e.g., cat: Aitkin et al. 1984; rabbit: Kuwada et al. 2011) although those same studies also report subpopulations of sharply tuned, level-tolerant units. The difference between species might be due to differences in the underlying anatomical circuitry of converging inputs to the IC. In rats, the commissure of the IC is thought to provide intensity-dependent excitatory and inhibitory input to most ICc neurons (Malmierca et al. 2005). Whether or not input from the intercollicular commissure varies between species remains to be seen. Despite the degraded spatial sensitivity in the ICc at higher sound levels, its two ascending targets showed sharp, level-tolerant spatial sensitivity. We hypothesize that the advent of level invariance in those targets represents changes in the balance of contralateral excitation and ipsilateral inhibition, but tests of that assumption must wait for future intracellular studies. The present extracellular data indicate that sharp spatial sensitivity arises in two distinct pathways, the tectal pathway through the BIN and the lemniscal pathway through the MGBv.

The BIN has been reported to receive direct projections from the ICc (Jiang et al. 1993; King et al. 1998; Nodal et al. 2005; Slee and Young 2013). All of our BIN units exhibited relatively sharp, level-tolerant spatial sensitivity that was biased to the contralateral hemifield (Fig. 9). As a result, these units were capable of discriminating nearly half of all azimuth locations across our tested sound levels (Fig. 8). Preference for contralateral azimuth locations is typically seen in the few studies that

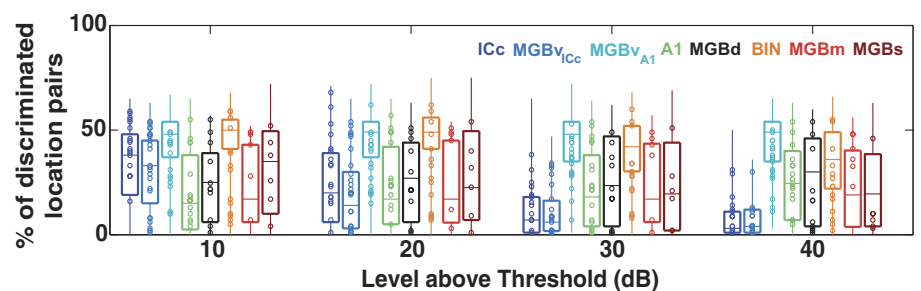


Fig. 8. Distributions of percentages of discriminated location pairs for all sampled populations as a function of level above threshold. Similar convention as in Fig. 6A.

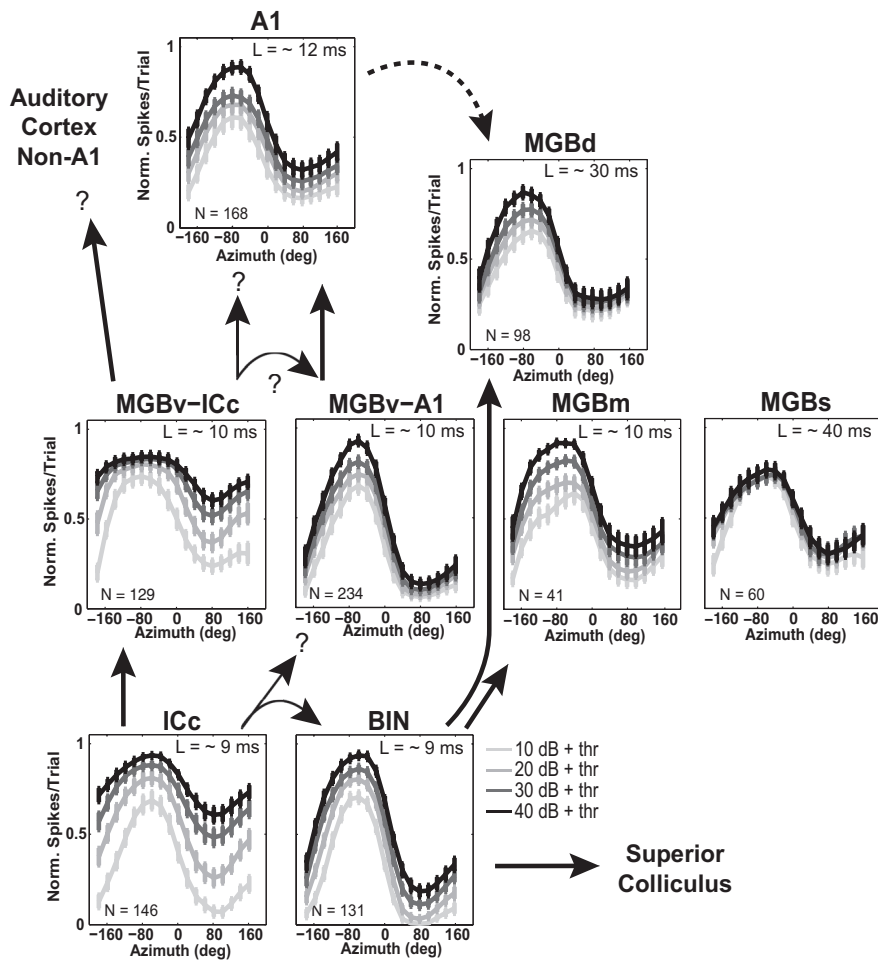


Fig. 9. Grand mean RAFs across 10, 20, 30, and 40 dB above threshold from all units within each subdivision sampled. RAFs are normalized to the maximum spike rate location and highest level of each unit. Data are presented along the ascending (solid lines) and descending (dashed lines) circuitry of the IC-MGB-A1 axis with possible inheritance and/or transformations from circuitry projections based on latency ( $L$ ). Notice the transformation of azimuth representation as it ascends from the ICc to MGBv and from the ICc to BIN.

examined the spatial sensitivity of this structure (ferret: Schnupp and King 1997; awake marmoset: Slee and Young 2013); however, we found spatial sensitivity in the rat to be much sharper than that seen in awake marmosets and more level-tolerant than in the ferret. The absence of BIN units showing broad spatial sensitivity in the present study suggests that the transformation to sharp spatial sensitivity in the BIN is complete at or before the level of synapses of ICc axons onto BIN neurons in the rat. In anesthetized ferrets, Schnupp and King (1997) found a rather indistinct topography of spatial tuning as a function of BIN location. We observed no such topography in the rat BIN, which is not surprising given the very limited range of spatial centroids in the rat BIN. Previous studies have shown that the BIN projects to the SC (ferret: Jiang et al. 1993; King et al. 1998). In the SC of the rat, neurons showed predominantly contralateral hemifield spatial sensitivity, and there was only a somewhat poorly defined spatial topography (Gaese and Johnen 2000). That is consistent with the notion that the spatial sensitivity seen in the SC is inherited largely from the BIN.

About 65% of the units in our sample of the MGBv units, the A1-like units, showed sharp, level-tolerant spatial sensitivity, whereas the other 35% showed broader spatial sensitivity (ICc-like), vulnerable to increasing sound level, like that observed in the ICc. The MGBv is well known to receive its ascending input from the principal cells in the ICc (Calford and Aitkin 1983). At present, it is not clear whether the sharply

tuned A1-like MGBv units that we studied were directly postsynaptic to ICc axons or whether they received their input by way of the MGBv-ICc-like neurons. That issue is considered in the following section.

#### Two Populations of Neurons Within the MGBv

An unexpected finding was that of the two distinct populations of neurons within the MGBv. The populations differed markedly in their spatial sensitivity while showing little or no differences in other physiological measures that we evaluated. We also observed a conspicuous nonrandom distribution of these two classes of neurons in the MGBv. The organization of adjacent units with similar spatial sensitivity is reminiscent of the complex banded organization of binaural sensitivity in the cat MGBv, where neurons that project to cortical neurons that are excited by either ear (EE) are segregated from those that project to cortical neurons that are inhibited by the ipsilateral ear (EI) (Middlebrooks and Zook 1983). EE and EI characteristics could be similarly compared with the broad spatial sensitivity of MGBv-ICc-like and the sharp spatial sensitivity of MGBv-A1-like units, respectively.

We consider two hypotheses for the origin of such distinct unit classes within the MGBv. One hypothesis is that MGBv-ICc-like units lie on a pathway between the ICc and MGBv-A1-like units, first receiving direct input from the ICc and then projecting to MGBv-A1-like units. If A1-like units received direct input from ICc-like units, then their response latencies

would be longer than those of ICc-like units. Contrary to that prediction, first-spike latencies of the MGBv-A1-like population were not significantly different from those of the MGBv-ICc-like population, arguing against such an anatomical substrate. An alternative hypothesis involves two distinct functional pathways, with MGBv-A1-like units resulting from a transformation of spatial sensitivity across the colliculo-thalamic synapse and MGBv-ICc-like units directly inheriting spatial sensitivity from the ICc.

One might raise the hypothesis that the ICc already contains both broadly and sharply tuned unit classes but that our use of multi-unit recording obscured the sharp tuning by recording simultaneously from putatively intermingled broadly and sharply tuned units. That hypothesis seems unlikely in that not one of the 17 well-isolated single units recorded in the ICc showed sharp, level-tolerant spatial sensitivity like that shown by the MGBv-A1-like units.

The anatomical projection sites of the two distinct classes of MGBv units are largely unknown. Our previous observations of sharp level-tolerant spatial tuning in rat A1 units would be consistent with the view that rat A1 spatial sensitivity is inherited exclusively from MGBv-A1-like units and that the MGBv-ICc-like units either project elsewhere in the cortex or do not project out of the MGB. Alternatively, it might be that A1-like and ICc-like projections are somehow combined but that the A1-like inputs dominate the spatial sensitivity seen in A1. One possible cortical projection target for MGBv-ICc-like units could be auditory areas anterior and posterior to A1, where units showing excitatory inputs from both ears have been reported (Kelly and Sally 1988). Future work involving anatomical and physiological methodology is needed to explore these hypotheses.

#### *Potential Behavioral Relevance for Parallel Pathways for Auditory Space Processing*

Previous studies suggest distinct roles of tectal and lemniscal pathways in auditory spatial behavior and perception. The tectal pathway provides auditory input to the SC for its role in directing reflexive orienting movements of the eyes, head, and external ears to auditory and multisensory stimuli (Sparks and Groh 1995; King 2004). Unilateral lesions of the SC in cats result in lengthening of the latencies of behavioral orientations to contralateral sounds (Thompson and Masterton 1978) and reduce the multisensory enhancement of orientation responses to spatially coincident auditory and visual targets (Burnett et al. 2004). In contrast, the lemniscal pathway has been shown in cats and ferrets to be essential for operant localization of sound sources, including responses to remembered locations. For example, unilateral lesions (Jenkins and Merzenich 1984) or inactivation by cortical cooling (Malhotra and Lomber 2007) of auditory cortex disrupts the ability of a cat to walk to the remembered location of a brief sound presented from the side contralateral to the lesion or inactivation. Similar dissociations of reflexive orientation and localization of remembered targets have been demonstrated in homologous tectal and lemniscal pathways in the barn owl (Knudsen and Knudsen 1996; Knudsen et al. 1993). Severe impairments in left vs. right discrimination ability were seen in rats when lesions were made within the tectal pathway (Kelly and Judge 1985), suggesting that left vs. right orientation ability requires an intact tectal pathway.

Consistent with these findings, our recorded BIN units could accurately discriminate between hemifield source locations, possessing percentages of discriminated location pairs around 50% (Fig. 8). It remains to be tested how transformation of spatial sensitivity along the lemniscal pathway aids in the perception of sound-source locations. Optogenetic and chemical genetic approaches may provide a means to directly assess this in future studies.

#### ACKNOWLEDGMENTS

We thank Zekiye Onsan, Lauren Javier, and Elizabeth McGuire for technical and administrative assistance. We also thank Minhan Dinh and Dr. Karina Cramer for generously providing advice, facilities, and supplies for histology.

#### GRANTS

The work is supported by National Institute on Deafness and Other Communication Disorders Grants RO1 DC000420 and F31 DC013013 (J. D. Yao).

#### DISCLOSURES

No conflicts of interest, financial or otherwise, are declared by the authors.

#### AUTHOR CONTRIBUTIONS

Author contributions: J.D.Y., P.B., and J.C.M. conception and design of research; J.D.Y. and P.B. performed experiments; J.D.Y. and P.B. analyzed data; J.D.Y., P.B., and J.C.M. interpreted results of experiments; J.D.Y. prepared figures; J.D.Y. drafted manuscript; J.D.Y., P.B., and J.C.M. edited and revised manuscript; J.D.Y., P.B., and J.C.M. approved final version of manuscript.

#### REFERENCES

- Aitkin LM, Gates GR, Phillips SC. Responses of neurons in inferior colliculus to variations in sound-source azimuth. *J Neurophysiol* 52: 1–17, 1984.
- Anderson LA, Linden JF. Physiological differences between histologically defined subdivisions in the mouse auditory thalamus. *Hear Res* 274: 48–60, 2011.
- Anderson LA, Wallace MN, Palmer AR. Identification of subdivisions in the medial geniculate body of the guinea pig. *Hear Res* 228: 156–167, 2007.
- Bartlett EL, Stark JM, Guillery RW, Smith PH. Comparison of the fine structure of cortical and collicular terminals in the rat medial geniculate body. *Neuroscience* 100: 811–828, 2000.
- Bauerle P, von der Behrens W, Kossel M, Gaese BH. Stimulus-specific adaptation in the gerbil primary auditory thalamus is the result of a fast frequency-specific habituation and is regulated by the corticofugal system. *J Neurosci* 31: 9708–9722, 2011.
- Bierer SM, Anderson DJ. Multi-channel spike detection and sorting using an array processing technique. *Neurocomputing* 26–27: 947–956, 1999.
- Bordi F, LeDoux JE. Response properties of single units in areas of rat auditory thalamus that project to the amygdala. I. Acoustic discharge patterns and frequency receptive fields. *Exp Brain Res* 98: 261–274, 1994a.
- Bordi F, LeDoux JE. Response properties of single units in areas of rat auditory thalamus that project to the amygdala. II. Cells receiving convergent auditory and somatosensory inputs and cells antidromically activated by amygdala stimulation. *Exp Brain Res* 98: 275–286, 1994b.
- Burnett LR, Stein BE, Chaponis D, Wallace MT. Superior colliculus lesions preferentially disrupt multisensory orientation. *Neuroscience* 124: 535–547, 2004.
- Calford MB, Aitkin LM. Ascending projections to the medial geniculate body of the cat: evidence for multiple, parallel auditory pathways through thalamus. *J Neurosci* 3: 2365–2380, 1983.
- Cetas JS, Price RO, Velenovsky DS, Crowe JJ, Sinex DG, McMullen NT. Cell types and response properties of neurons in the ventral division of the medial geniculate body of the rabbit. *J Comp Neurol* 445: 78–96, 2002.

- de Venecia RK, Smelser CB, Lossman SD, McMullen NT. Complementary expression of parvalbumin and calbindin D-28k delineates subdivisions of the rabbit medial geniculate body. *J Comp Neurol* 359: 595–612, 1995.
- de Venecia RK, Smelser CB, McMullen NT. Parvalbumin is expressed in a reciprocal circuit linking the medial geniculate body and auditory neocortex in the rabbit. *J Comp Neurol* 400: 349–362, 1998.
- DiCarlo JJ, Lane JW, Hsiao SS, Johnson KO. Marking microelectrode penetrations with fluorescent dyes. *J Neurosci Methods* 64: 75–81, 1996.
- Edeline JM, Manunta Y, Nodal FR, Bajo VM. Do auditory responses recorded from awake animals reflect the anatomical parcellation of the auditory thalamus? *Hear Res* 131: 135–152, 1999.
- Ernst MD. Permutation methods: a basis for exact inference. *Stat Sci* 19: 676–685, 2004.
- Gaese BH, Johnen A. Coding for auditory space in the superior colliculus of the rat. *Eur J Neurosci* 12: 1739–1752, 2000.
- Green DM, Swets JA. *Signal Detection Theory and Psychophysics*. New York, NY: Wiley, 1966.
- Grothe B, Pecka M, McAlpine D. Mechanisms of sound localization in mammals. *Physiol Rev* 90: 983–1012, 2010.
- Hackett TA, Barkat TR, O'Brien BM, Hensch TK, Polley DB. Linking topography to tonotopy in the mouse auditory thalamocortical circuit. *J Neurosci* 31: 2983–2995, 2011.
- Hashikawa T, Rausell E, Molinari M, Jones EG. Parvalbumin- and calbindin-containing neurons in the monkey medial geniculate complex: differential distribution and cortical layer specific projections. *Brain Res* 544: 335–341, 1991.
- Hazama M, Kimura A, Donishi T, Sakoda T, Tamai Y. Topography of corticothalamic projections from the auditory cortex of the rat. *Neuroscience* 124: 655–667, 2004.
- He J. On and off pathways segregated at the auditory thalamus of the guinea pig. *J Neurosci* 21: 8672–8679, 2001.
- He J, Hu B. Differential distribution of burst and single-spike responses in auditory thalamus. *J Neurophysiol* 88: 2152–2156, 2002.
- Jenkins WM, Merzenich MM. Role of cat primary auditory cortex for sound-localization behavior. *J Neurophysiol* 52: 819–847, 1984.
- Jiang ZD, King AJ, Moore DR. Topographic projection from the brachium of the inferior colliculus to the space mapped region of the superior colliculus in the ferret. *Br J Audiol* 27: 344–345, 1993.
- Kavanagh GL, Kelly JB. Midline and lateral field sound localization in the albino rat (*Rattus norvegicus*). *Behav Neurosci* 100: 200–205, 1986.
- Kelly JB, Judge PW. Effects of medial geniculate lesions on sound localization by the rat. *J Neurophysiol* 53: 361–372, 1985.
- Kelly JB, Sally SL. Organization of auditory cortex in the albino rat: binaural response properties. *J Neurophysiol* 59: 1756–1769, 1988.
- King AJ. The superior colliculus. *Curr Biol* 14: R335–R338, 2004.
- King AJ, Hutchings ME. Spatial response properties of acoustically responsive neurons in the superior colliculus of the ferret: a map of auditory space. *J Neurophysiol* 57: 596–624, 1987.
- King AJ, Middlebrooks JC. Cortical representation of auditory space. In: *The Auditory Cortex*, edited by Winer J and Schreiner C. New York, NY: Springer, 2011, pp. 329–341.
- King AJ, Jiang ZD, Moore DR. Auditory brainstem projections to the ferret superior colliculus: anatomical contribution to the neural coding of sound azimuth. *J Comp Neurol* 390: 342–365, 1998.
- Knudsen EI, Knudsen PF. Disruption of auditory spatial working memory by inactivation of the forebrain archistriatum in barn owls. *Nature* 383: 428–431, 1996.
- Knudsen EI, Knudsen PF, Masino T. Parallel pathways mediating both sound localization and gaze control in the forebrain and midbrain of the barn owl. *J Neurosci* 13: 2837–2852, 1993.
- Koka K, Read HL, Tollin DJ. The acoustical cues to sound location in the rat: measurements of directional transfer functions. *J Acoust Soc Am* 123: 4297–4309, 2008.
- Kudo M, Tashiro T, Higo S, Matsuyama T, Kawamura S. Ascending projections from the nucleus of the brachium of the inferior colliculus in the cat. *Exp Brain Res* 54: 203–211, 1984.
- Kuwada S, Bishop B, Alex C, Condit DW, Kim DO. Spatial tuning to sound-source azimuth in the inferior colliculus of unanesthetized rabbit. *J Neurophysiol* 106: 2698–2708, 2011.
- Kyweriga M, Stewart W, Cahill C, Wehr M. Synaptic mechanisms underlying interaural level difference selectivity in rat auditory cortex. *J Neurophysiol* 112: 2561–2571, 2014.
- Lee CC, Middlebrooks JC. Auditory cortex spatial sensitivity sharpens during task performance. *Nat Neurosci* 14: 108–114, 2011.
- Lumani A, Zhang H. Responses of neurons in the rat's dorsal cortex of the inferior colliculus to monaural tone bursts. *Brain Res* 1351: 115–129, 2010.
- Macmillan NA, Creelman CD. *Detection Theory: A User's Guide*, Ed. 2. Mahwah, NJ: Lawrence Erlbaum, 2005.
- Malhotra S, Lomber SG. Sound localization during homotopic and heterotopic bilateral cooling deactivation of primary and nonprimary auditory cortical areas in the cat. *J Neurophysiol* 97: 26–43, 2007.
- Malmierca MS, Hernandez O, Rees A. Intercollicular commissural projections modulate neuronal responses in the inferior colliculus. *Eur J Neurosci* 21: 2701–2710, 2005.
- Malmierca MS, Izquierdo MA, Cristaudo S, Hernandez O, Perez-Gonzalez D, Covey E, Oliver DL. A discontinuous tonotopic organization in the inferior colliculus of the rat. *J Neurosci* 28: 4767–4776, 2008.
- Middlebrooks JC. Auditory cortex phase locking to amplitude-modulated cochlear implant pulse trains. *J Neurophysiol* 100: 76–91, 2008.
- Middlebrooks JC, Bremen P. Spatial stream segregation by auditory cortical neurons. *J Neurosci* 33: 10986–11001, 2013.
- Middlebrooks JC, Knudsen EI. A neural code for auditory space in the cat's superior colliculus. *J Neurosci* 4: 2621–2634, 1984.
- Middlebrooks JC, Snyder RL. Auditory prosthesis with a penetrating nerve array. *J Assoc Res Otolaryngol* 8: 258–279, 2007.
- Middlebrooks JC, Zook JM. Intrinsic organization of the cat's medial geniculate body identified by projections to binaural response-specific bands in the primary auditory cortex. *J Neurosci* 3: 203–224, 1983.
- Middlebrooks JC, Xu L, Eddins AC, Green DM. Codes for sound-source location in nontotopic auditory cortex. *J Neurophysiol* 80: 863–881, 1998.
- Nodal FR, Doubell TP, Jiang ZD, Thompson ID, King AJ. Development of the projection from the nucleus of the brachium of the inferior colliculus to the superior colliculus in the ferret. *J Comp Neurol* 485: 202–217, 2005.
- Palmer AR, King AJ. The representation of auditory space in the mammalian superior colliculus. *Nature* 299: 248–249, 1982.
- Patterson RD. Auditory filter shapes derived with noise stimuli. *J Acoust Soc Am* 59: 640–654, 1976.
- Paxinos G, Watson C. *The Rat Brain in Stereotaxic Coordinates*. Burlington, VT: Elsevier-Academic, 2005.
- Read HL, Miller LM, Schreiner CE, Winer JA. Two thalamic pathways to primary auditory cortex. *Neuroscience* 152: 151–159, 2008.
- Redies H, Brandner S, Creutzfeldt OD. Anatomy of the auditory thalamocortical system of the guinea pig. *J Comp Neurol* 282: 489–511, 1989.
- Rouiller EM, Welker E. Morphology of corticothalamic terminals arising from the auditory cortex of the rat: a Phaseolus vulgaris-leucoagglutinin (PHA-L) tracing study. *Hear Res* 56: 179–190, 1991.
- Schnupp JW, King AJ. Coding for auditory space in the nucleus of the brachium of the inferior colliculus in the ferret. *J Neurophysiol* 78: 2717–2731, 1997.
- Shi CJ, Cassell MD. Cortical, thalamic, and amygdaloid projections of rat temporal cortex. *J Comp Neurol* 382: 153–175, 1997.
- Slee SJ, Young ED. Linear processing of interaural level difference underlies spatial tuning in the nucleus of the brachium of the inferior colliculus. *J Neurosci* 33: 3891–3904, 2013.
- Sparks DL, Groh JM. The superior colliculus: a window for viewing issues in integrative neuroscience. In: *The Cognitive Neurosciences*, edited by Gazzaniga MS. Cambridge, MA: MIT, 1995, pp. 565–584.
- Syka J, Popelar J, Kvasnak E, Astl J. Response properties of neurons in the central nucleus and external and dorsal cortices of the inferior colliculus in guinea pig. *Exp Brain Res* 133: 254–266, 2000.
- Thompson GC, Masterton RB. Brainstem auditory pathways involved in reflexive head orientation to sound. *J Neurophysiol* 41: 1183–1202, 1978.
- Verschooten E, Robles L, Kovacic D, Joris PX. Auditory nerve frequency tuning measured with forward-masked compound action potentials. *J Assoc Res Otolaryngol* 13: 799–817, 2012.
- Winer JA, Diehl JJ, Larue DT. Projections of auditory cortex to the medial geniculate body of the cat. *J Comp Neurol* 430: 27–55, 2001.
- Yao JD, Bremen P, Middlebrooks JC. Rat primary auditory cortex is tuned exclusively to the contralateral hemifield. *J Neurophysiol* 110: 2140–2151, 2013.
- Zhou B, Green DM, Middlebrooks JC. Characterization of external ear impulse responses using Golay codes. *J Acoust Soc Am* 92: 1169–1171, 1992.